# Protonation, Tautomerization, and Rotameric Structure of Histidine: A Comprehensive Study by Magic-Angle-Spinning Solid-State NMR

Shenhui Li and Mei Hong*

Department of Chemistry, Iowa State University, Ames, Iowa 50011, United States

S *Supporting Information*

ABSTRACT: Histidine structure and chemistry lie at the heart of many enzyme active sites, ion channels, and metalloproteins. While solid-state NMR spectroscopy has been used to study histidine chemical shifts, the full pH dependence of the complete panel of ^{15}N, ^{13}C, and ^{1}H chemical shifts and the sensitivity of these chemical shifts to tautomeric structure have not been reported. Here we use magic-angle-spinning solid-state NMR spectroscopy to determine the ^{15}N, ^{13}C, and ^{1}H chemical shifts of histidine from pH 4.5 to 11. Two-dimensional homonuclear and heteronuclear correlation spectra indicate that these chemical shifts depend sensitively on the protonation state and tautomeric structure. The chemical shifts of the rare π tautomer were observed for the first time, at the most basic pH used. Intra- and intermolecular hydrogen bonding between the imidazole nitrogens and the histidine backbone or water was detected, and N—H bond length measurements indicated the strength of the hydrogen bond. We also demonstrate the accurate measurement of the histidine side-chain torsion angles χ_1 and χ_2 through backbone—side chain $^{13}C-^{15}N$ distances; the resulting torsion angles were within 4° of the crystal structure values. These results provide a comprehensive set of benchmark values for NMR parameters of histidine over a wide pH range and should facilitate the study of functionally important histidines in proteins.
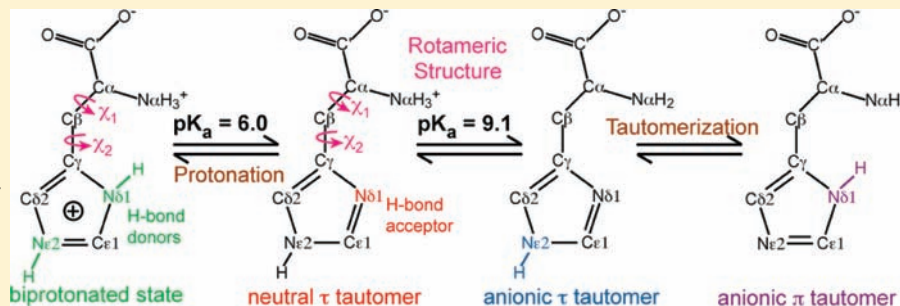
■ INTRODUCTION

Histidine is an essential amino acid whose side-chain pK_a (∼6) is closest, among all amino acids, to the physiological pH. Thus, small changes in the environmental pH can readily change the histidine charged state. At low pH, both imidazole nitrogens are protonated to give the cationic imidazolium. Near pH 7, two neutral tautomers exist: the $N\varepsilon2$-protonated τ tautomer and the $N\delta1$-protonated π tautomer. At mildly basic pH, the backbone $N\alpha$ becomes deprotonated to give an anionic histidine, whose side chain is neutral in either tautomeric state. At even higher pH or when complexed with metal ions, the imidazole can lose another proton to give an imidazolate ion.[1,2] Neutral histidine can serve as a general base and a common coordinating ligand for transition metals, while cationic histidine can serve as a general acid and hydrogen-bond (H-bond) donor. Because of its rich chemistry and pH sensitivity in the physiologically relevant range, histidine is found in the active sites of many proteins and plays key roles in enzyme catalysis,[3,4] proton conduction,[5,6] proton pumps,[7] photosynthetic complexes,[8] and metalloproteins.[9,10] In addition to protonation chemistry and metal coordination, the neutral imidazole of histidine can combine tautomerization with ring flips (180° χ_2 angle changes) to interconvert the protonated and unprotonated nitrogens without significantly changing the space occupied by the ring. Thus, histidine side-chain rotamerization is often important for protein function.[11]

A number of NMR investigations of the chemical structure and dynamics of histidine in proteins have been reported. For example, de Groot and co-workers studied the interactions of histidines in the light-harvesting complex II with bacteriochlorophyll and found that $N\varepsilon2$ was ligated with Mg^{2+} while $N\delta1$ was protonated and involved in H-bonding.[12] Kay and co-workers[13] investigated the interconversion of His61 in plastocyanin of *Anabana variabilis* among three tautomeric and protonated states. Cross and co-workers[14] characterized the protonation state of the histidine responsible for the activation of the influenza A M2 proton channel and found the charged state of the tetrad that coincides with channel opening.

A number of solid-state NMR studies of histidine and imidazole ^{13}C and ^{15}N chemical shifts and bond lengths have also been reported. ^{15}N isotropic and anisotropic chemical shifts have been used to characterize the acid—base and tautomeric equilibria of histidine.[15,16] The δ_{22} principal value of the ^{15}N chemical shielding tensor in the cationic imidazolium was found to depend on the H-bond length.[17] A linear correlation was observed between the

imidazole ^{15}N isotropic chemical shift and the degree of N—H bond stretching due to H-bonding.[18] The imidazole ^{13}C chemical shifts of histidine lyophilized from solutions of varying pH were also found to contain information on the pK_a of the parent solution.[19] Quantum chemical calculations showed that the Cγ and C$\delta 2$ chemical shifts were highly correlated and depended on the tautomeric structure.[20]

Despite these extensive investigations, so far no studies have provided a complete set of ^{15}N, ^{13}C, and ^{1}H chemical shifts of histidine and its H-bonding properties and rotameric conformations over a wide range of pH values. Moreover, the minor π tautomer has not been observed in small-molecule histidine compounds. Most solid-state NMR studies used site-specifically ^{15}N-labeled samples with ^{13}C in natural abundance, making it difficult to correlate the ^{13}C, ^{15}N, and ^{1}H chemical shifts. To facilitate structure determination of histidines in protein active sites, we thus carried out a comprehensive study of the NMR structural parameters of histidine as a function of pH using magic-angle-spinning (MAS) NMR techniques. ^{15}N, ^{13}C, and ^{1}H isotropic chemical shifts and ^{15}N chemical shift anisotropies were measured from pH 4.5 to 11 on uniformly ^{13}C,^{15}N-labeled histidine and its salts. This pH range allowed us to detect four protonation states of histidine and both the major τ tautomer and the minor π tautomer, the latter being observed for the first time. We also investigated intra- and intermolecular H-bonding through ^{1}H chemical shifts and N—H bond stretching effects. Finally, we demonstrate that χ_1 and χ_2 torsion angles indicative of the side-chain rotameric conformation can be measured accurately from backbone—side chain ^{13}C—^{15}N distances.

■ METHODS AND MATERIALS

Sample Preparation. ^{13}C,^{15}N-Labeled (98%) histidine hydrochloride monohydrate was purchased from Sigma-Aldrich and was recrystallized in aqueous solutions of various pH to obtain histidine samples at pH 4.5, 6.0, 8.5, and 11.0. About 30 mg of the labeled histidine powder was dissolved in 600 μL of solution, the pH of which was adjusted by mixing appropriate volumes of 1 M HCl and NaOH. The solution pH was verified by pH paper to a precision of ±0.5. The four samples were designated as His4.5, His6.0, His8.5, and His11.0. The solutions were slowly dried at ambient temperature in 3—5 days to obtain microcrystalline powders, which were then packed into 4 mm MAS rotors for NMR experiments. For distance experiments to determine the side-chain conformation, it was necessary to remove the effects of intermolecular dipolar couplings. To achieve this we diluted the ^{13}C,^{15}N-labeled histidine to 20% by co-dissolving it with 80% unlabeled histidine hydrochloride monohydrate. Two diluted samples were prepared at pH 4.5 and 8.0.

Solid-State NMR Spectroscopy. Solid-state NMR experiments were carried out on a wide-bore Bruker AVANCE-600 spectrometer (14.1 T) and a DSX-400 spectrometer (Karlsruhe, Germany) on 4-mm triple-resonance MAS probes. Typical radiofrequency field strengths were 35—50 kHz for ^{13}C and ^{15}N and 62—83 kHz for ^{1}H. ^{13}C chemical shifts were referenced to the α-Gly C′ signal at 176.49 ppm on the TMS scale and ^{15}N chemical shifts were referenced to the ^{15}N signal of N-acetylvaline at 122 ppm on the liquid ammonia scale. The ^{1}H chemical shifts were externally referenced to those of N-formyl-U-^{13}C,^{15}N-labeled Met-Leu-Phe-OH .[21]

Three types of 2D correlation experiments were used to determine the ^{13}C, ^{15}N, and ^{1}H isotropic chemical shifts. 2D ^{13}C—^{13}C DARR correlation experiments[22] were carried out with a 5 ms mixing time under 9 kHz MAS. 2D ^{15}N—^{13}C correlation spectra[23] were measured under 9 kHz MAS using a REDOR[24] pulse train of 0.44 ms for ^{13}C—^{15}N coherence transfer. 2D ^{1}H—^{15}N and ^{1}H—^{13}C heteronuclear correlation

(HETCOR) experiments were carried out with Lee—Goldburg (LG)[25] cross-polarization (CP) from ^{1}H, and the samples were spun at 7.5 kHz. The LG-CP contact time was 800 μs for ^{1}H—^{15}N and 300 μs for ^{1}H—^{13}C HETCOR experiments. ^{1}H homonuclear decoupling during the t_1 dimension was achieved using the FSLG pulse sequence[26] with a transverse ^{1}H field strength of 80 kHz.

To identify histidine—water intermolecular contacts, we carried out a ^{1}H—^{15}N 2D HETCOR experiment with a MELODI dipolar filter,[27,28] where two rotor periods of ^{13}C and ^{15}N dipolar dephasing were added before the ^{1}H evolution period. These ^{15}N-detected MELODI-HETCOR experiments used a Hartmann—Hahn CP contact time of 3 ms, and the sample was spun at 6859 Hz.

^{15}N chemical shift anisotropy (CSA) was measured using the 2D SUPER experiment[29] under slow spinning speeds of 3.0 and 3.6 kHz. The field strength of the ^{15}N CSA recoupling pulse was 36.4 and 43.6 kHz to satisfy the $\omega_1 = 12.12\omega_r$ recoupling condition. A ^{1}H decoupling field of 80 kHz and a ^{13}C decoupling pulse of 3 kHz were applied during ^{15}N t_1 evolution. The recoupled ^{15}N CSA powder patterns in the indirect dimension of the 2D spectra gave the three principal values δ_{ii}, from which the anisotropy parameter δ and the asymmetry parameter η were calculated using the following equations:

$$\delta \equiv \delta_{zz} - \delta_{iso} \tag{1}$$

$$\eta \equiv \frac{\delta_{yy} - \delta_{xx}}{\delta_{zz} - \delta_{iso}}, \text{ where } |\delta_{yy} - \delta_{iso}| \leq |\delta_{xx} - \delta_{iso}| \leq |\delta_{zz} - \delta_{iso}| \tag{2}$$

Another parameter describing the size of the CSA, the span $\Delta\sigma \equiv \delta_{11} - \delta_{33}$, was also calculated.

^{15}N—^{1}H dipolar couplings were measured using the dipolar-doubled DIPSHIFT experiment[30] under 4 kHz MAS. The time domain data were fit to give the apparent dipole coupling strengths and were divided by (2×0.54) to account for the dipolar doubling and the FSLG scaling factor to obtain the true coupling strength. The FSLG scaling factor of 0.54 was measured directly by comparing the ^{1}H chemical shifts of the 1D ^{1}H spectrum and the indirect dimension of the 2D ^{1}H—^{13}C HETCOR spectrum of methylmalonic acid, where the FSLG decoupling condition was the same as for histidine.

Intramolecular ^{13}C—^{15}N distances were measured on 20% diluted His4.5 and His8.0 samples to determine the rotameric structure. These distances were measured using the frequency-selective (FS) REDOR experiment[31] with ^{13}C detection and ^{15}N dephasing. For the ^{15}N inversion pulses every half a rotor period, composite 90°180°90° pulses were used to reduce the effects of flip angle errors and enhance the distance accuracy.[32] During the REDOR mixing period, 75—83 kHz of ^{1}H TPPM decoupling was applied, and the ^{15}N rf field strength was 36 kHz. A pair of soft Gaussian ^{13}C and ^{15}N inversion pulses were applied in the middle of the REDOR mixing period to selectively invert the peaks of interest. The Gaussian pulse lengths were rotor-synchronized to be 2 ms for ^{13}C and 4 ms for ^{15}N. The long ^{15}N soft pulse was necessary to selectively invert the N$\delta 1$ and N$\varepsilon 2$ peaks in the pH 4.5 sample, since the two peaks differ by only 14 ppm. For each REDOR mixing time (t_m), a control spectrum (S_0) with the central ^{15}N Gaussian pulse off and a dephasing spectrum (S) with the ^{15}N Gaussian pulse on were measured. The intensity $\Delta S/S_0 \equiv (S_0 - S)/S_0$ as a function of t_m gives the ^{13}C—^{15}N dipolar coupling. The FS-REDOR experiments were carried out under 7 kHz MAS. In simulating the REDOR data, we corrected for the presence of natural-abundance ^{13}C and ^{15}N spins according to

$$\left[1 - \left(\frac{S}{S_0}\right)_{obs}\right] = 93.8\% \times 1 - \left(\frac{S}{S_0}\right)_{true, 100\%} \tag{3}$$

REDOR dephasing curves were simulated using the SIMPSON program.[33] The ^{15}N CSA was not included for protonated nitrogens, since they are sufficiently small to cause no detectable changes in the REDOR dephasing curves. For the N$\delta 1$ of the neutral τ tautomer, which exhibited the
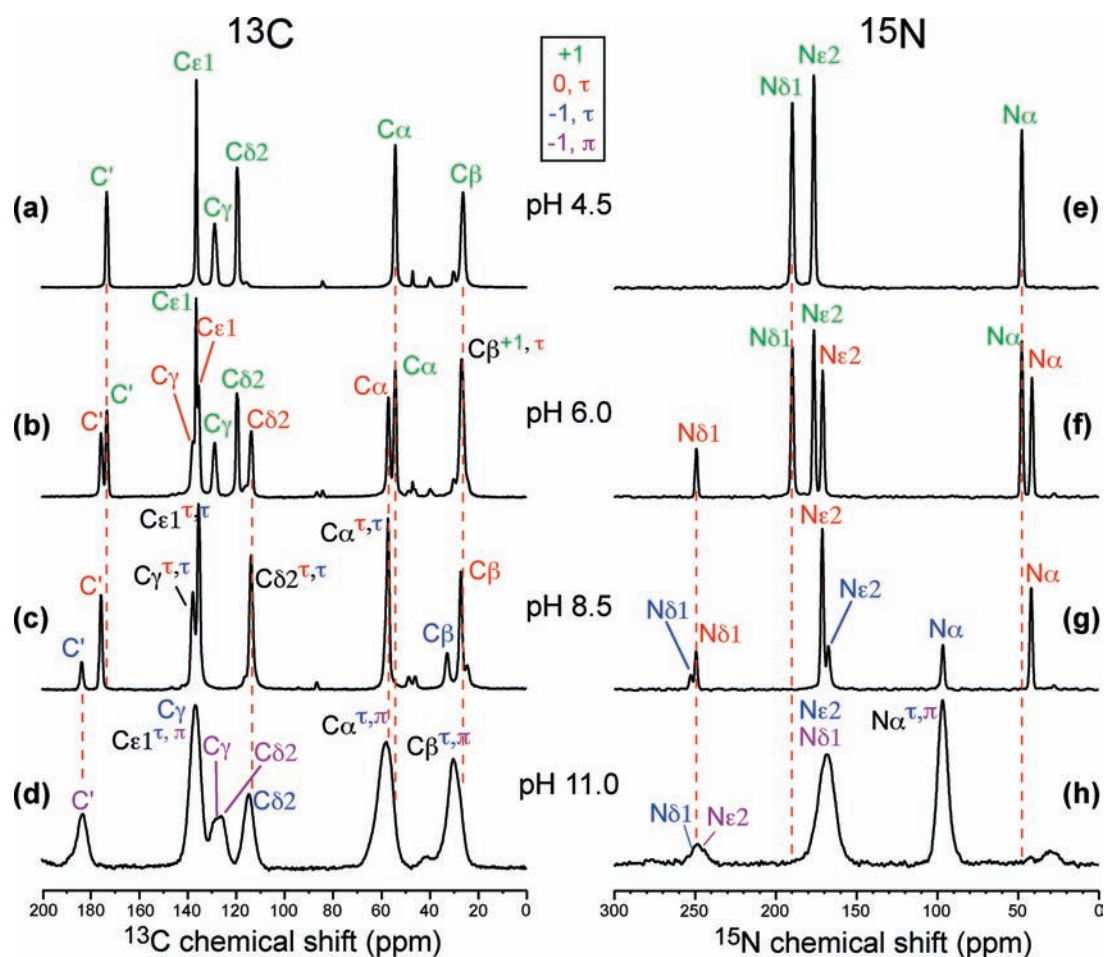
Figure 1. ^{13}C (left) and ^{15}N (right) CP-MAS spectra of histidine at pH 4.5 (a,e), 6.0 (b,f), 8.5 (c,g), and 11.0 (d,f). Peak assignments were obtained from 2D correlation spectra shown in Figure 2 and are color-coded as shown in the box. Assignment in black indicates a mixture of two different tautomeric or charged states of histidine.

largest ^{15}N CSA among all sites ($\delta = 210$ ppm, Table 2), the ^{15}N CSA was included in the simulation. The Nδ1 chemical shift tensor orientation was taken from ref 34, with Euler angles of 153°, 77°, and 101°, to describe the Cα–Nδ1 vector orientation in the Nδ1 chemical shift tensor frame.

RESULTS AND DISCUSSION

^{13}C and ^{15}N Isotropic Chemical Shifts. To determine the protonation and tautomeric structure of histidine, we measured the ^{13}C and ^{15}N chemical shifts of histidine. Figure 1 shows 1D ^{13}C and ^{15}N CP-MAS spectra of histidine from pH 4.5 to 11.0. In this paper, we use green to designate the low-pH biprotonated and cationic histidine, red for the neutral τ tautomer, blue for the backbone anionic τ tautomer, and purple for the backbone anionic π tautomer. Figure 1 shows that both backbone and side-chain chemical shifts vary with the pH of the solution from which the samples were prepared. For the pH 4.5 sample, the ^{15}N isotropic shifts of both Nδ1 and Nϵ2 lie between 170 and 190 ppm, consistent with a biprotonated imidazolium, and no signal at the unprotonated ^{15}N chemical shift of ~250 ppm was observed. For all other pH states, the unprotonated ^{15}N signal was present. The Nα chemical shift reflects the charged state of the amino acid backbone. At pH 4.5 and 6.0, only an NH_3^+ peak at ~45 ppm was detected, while at pH 8.5 and 11, a 100 ppm ^{15}N NH_2 peak,

characteristic of an anionic backbone, was also present. At pH 11, this NH_2 peak was the dominant Nα signal.

The spectral line widths of the histidines were narrow between pH 4.5 and 8.5 but significantly broadened at pH 11. Below pH 9, the line widths were 1.3 ± 0.4 ppm for ^{13}C and 1.9 ± 0.2 ppm for ^{15}N, but at pH 11 the line widths increased to 5.5 ± 1.1 ppm for ^{13}C and 9.3 ± 2.2 ppm for ^{15}N (Figure 1d,h). The broader line widths indicate that the crystal packing was disrupted due to the coexistence of the τ and π tautomers. This is interesting because the rare π tautomer had not been detected in previous NMR studies of small histidine compounds at less basic pH conditions,[19] suggesting that the Nδ1-protonated π tautomer may be stabilized by intermolecular interactions with other imidazole rings.

Assignment of the ^{13}C and ^{15}N signals in Figure 1 was made using 2D ^{13}C–^{13}C and ^{15}N–^{13}C correlation experiments (Figure 2). A short mixing time of 5 ms was used for the ^{13}C–^{13}C DARR experiment to confine cross peaks mostly to one- and two-bond correlations. Figure 2a,b shows the full 2D ^{13}C–^{13}C and ^{15}N–^{13}C correlation spectra of His6.0, and Figure 2c,d shows the spectra of His11. A comparison of the aromatic side-chain region of the 2D ^{13}C–^{13}C spectra for all four pH's is given in Figure 2e, and Figure 2f shows the 2D ^{15}N–^{13}C HETCOR spectra of His4.5 and His8.5.

While only cationic histidine was present at pH 4.5, both cationic (green) and neutral τ tautomer (red) of histidine were
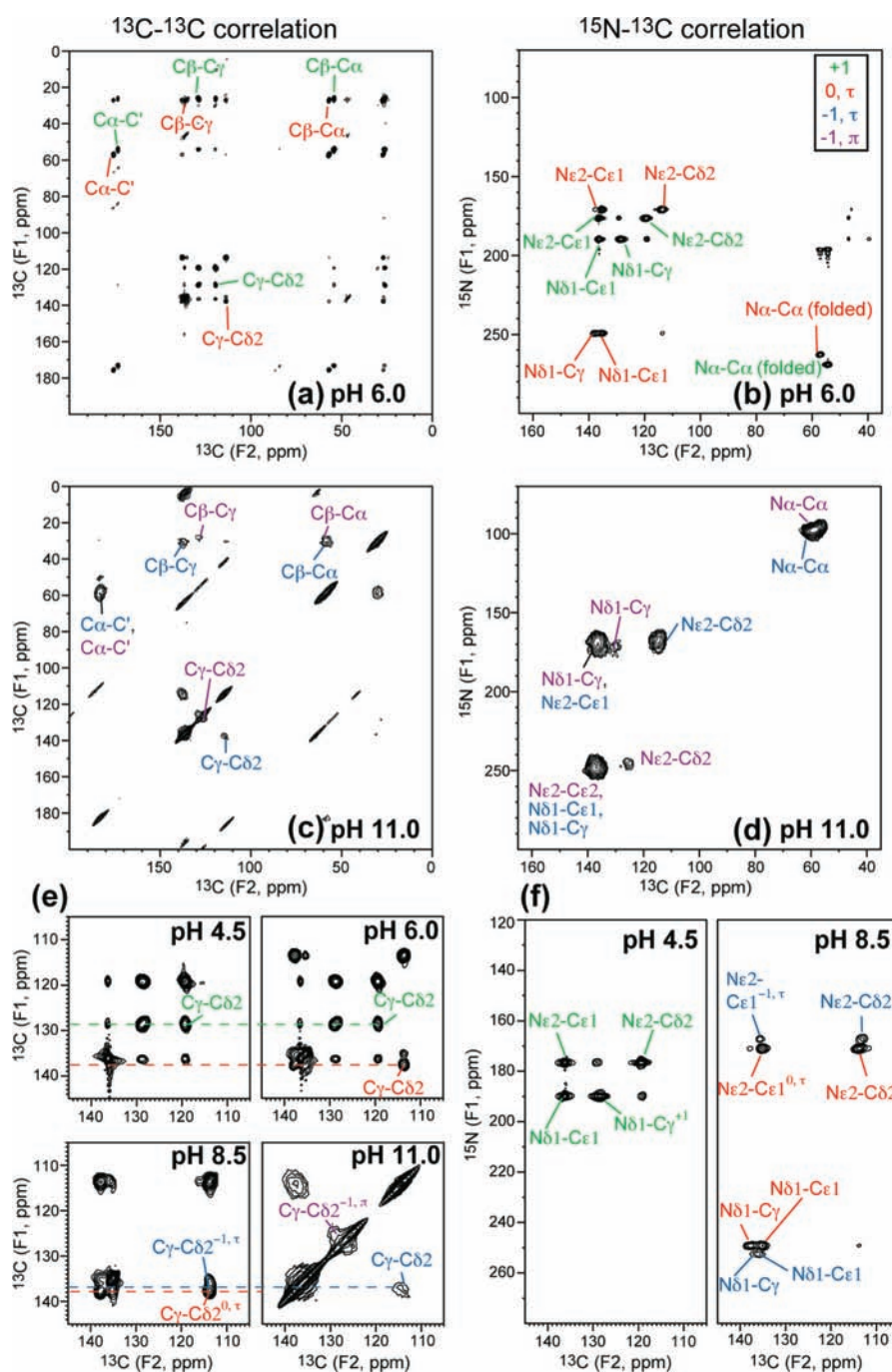
Figure 2. Representative 2D $^{13}C-^{13}C$ (a,c,e) and $^{15}N-^{13}C$ (b,d,f) correlation spectra of histidine from pH 4.5 to 11.0: (a,b) His6.0; (c,d) His11.0; (e) imidazole regions of the 2D $^{13}C-^{13}C$ correlation spectra of histidine; (f) imidazole side-chain regions of the 2D $^{15}N-^{13}C$ correlation spectra of His4.5 and His8.5.

observed as the pH increased to 6. The latter was evidenced by the Nδ1 peak at 249.4 ppm (Figure 2b). The ^{13}C chemical shifts nicely distinguish the cationic and neutral histidines. For example, the Cγ−Cδ2 cross peak resonated at (128.7, 119.4) ppm in the cationic state but shifted to (137.7, 113.6) ppm in the neutral τ tautomer. The backbone Cα, C′, and Nα chemical shifts also differed between the cationic histidine and the neutral τ tautomer. At pH 6, the intensity ratio of the cationic to the neutral histidine is about 54:46 (Figure 1b,f), consistent with the side-chain pK_a[16] of about 6 in aqueous solution (Scheme 1).

At pH 8.5, τ tautomers with a neutral backbone (red) and an anionic backbone (blue) coexisted at a ratio of about 3:1 (Figure 1c,g), in good agreement with the pK_a of 9.1 for the backbone amino group (Scheme 1). The absence of the π tautomer indicates that the τ tautomer is much more stable at pH 8.5, possibly due to intramolecular H-bonding. As the pH increased to 11, the neutral τ tautomer disappeared, and a second anionic histidine with a π tautomer (purple) was observed (Figure 2c,d). The pronounced line broadening of the spectra was directly related to the coexistence of the π and τ tautomers in the dry sample,
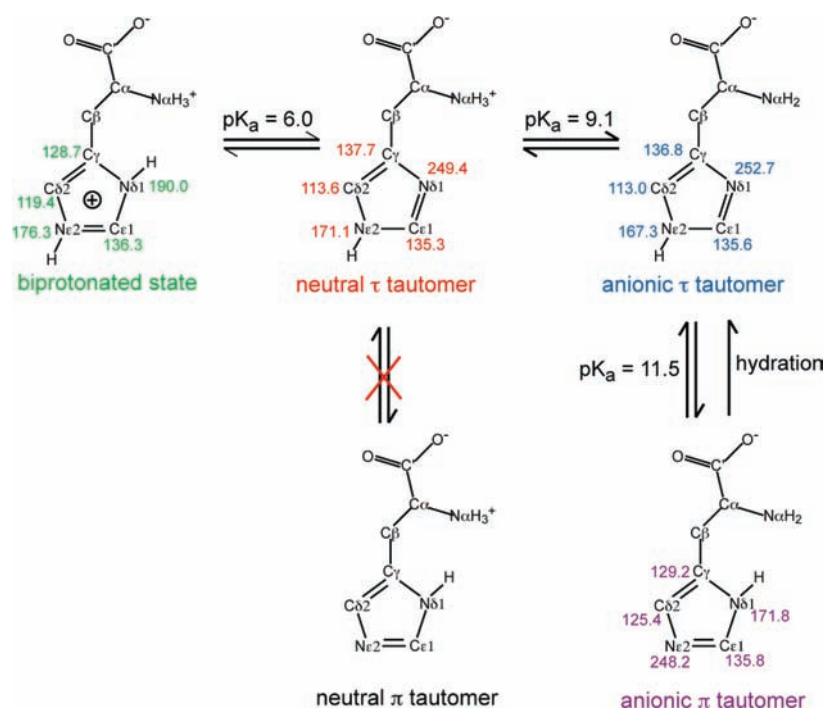
Scheme 1

Table 1. ^{1}H, ^{13}C, and ^{15}N Isotropic Chemical Shifts (ppm) of Histidine in Different Protonation and Tautomeric States

	site	cationic	neutral τ tautomer	anionic τ tautomer	anionic π tautomer
^{13}C	C′	173.2	175.6	183.4	183.2
	Cα	54.1	57.0	58.0	59.4
	Cβ	26.0	27.0	32.6	28.4
	Cγ	128.7	137.7	136.8	129.2
	Cε1	136.3	135.3	135.6	135.8
	Cδ2	119.4	113.6	113.0	125.4
^{15}N	Nα	47.6	41.5	96.3	96.3
	Nδ1	190.0	249.4	252.7	171.8
	Nε2	176.3	171.1	167.3	248.2
^{1}H	H^{N}	8.6	9.0	7.4	6.2
	Hα	3.5	4.3	5.2	4.0
	Hβ	3.3	2.7	2.7	2.7
	Hδ1	16.8	NA	NA	12.7
	Hε2	12.6	13.7	12.2	NA
	Hδ2	8.0	4.9	5.3	6.4
	Hε1	9.3	6.1	5.6	7.2

whose poor packing caused inhomogeneous local environments. When the sample was well hydrated at the same pH, we found that the anionic π tautomer transformed to the τ tautomer with concomitant line narrowing (Figure S1, Supporting Information). Thus, the anionic π tautomer is metastable and only found in the absence of water, suggesting that water–histidine H-bonding stabilizes the τ tautomer, which in turn implies that increased

percentages of the π tautomer in proteins must result from other stabilizing interactions, such as H-bonding with neighboring residues or coordination by metal ions.[20,35] The ^{13}C and ^{15}N isotropic chemical shifts of all four histidines are summarized in Table 1.

^{15}N Chemical Shift Anisotropies. Chemical shift anisotropy gives more complete information than isotropic shifts on the local electronic environment and on H-bonding.[17,20,34,36] Since the ^{13}C and ^{15}N isotropic chemical shifts already vary systematically with the protonation and tautomeric structure of the imidazole, the anisotropic chemical shifts are expected to show even larger variations. We measured the ^{15}N CSA of Nδ1 and Nε2 as a function of pH using the 2D SUPER experiment,[29] where the CSA line shapes were recoupled in the indirect dimension and separated according to their isotropic shifts in the direct dimension. While some of these ^{15}N CSAs were reported before,[15–17] the CSAs for the minor π tautomers were not known. Figure S2 (Supporting Information) shows the recoupled CSA patterns of Nδ1 and Nε2 at the four pH values. The three principal values, δ_{11}, δ_{22}, and δ_{33}, defined from the most downfield (left) to the most upfield chemical shifts, were directly read from the two edges and the maximum of the powder patterns. It can be seen that the protonated nitrogens exhibit smaller CSAs than unprotonated nitrogens. The span $\Delta\sigma$ ranges from 180 to 210 ppm (Table 2), in good agreement with literature values.[15,17] The protonated nitrogens in the cationic imidazolium have the upper bound of ∼210 ppm, whereas those in the neutral imidazoles adopt lower-bound values of 180–190 ppm. These spans are moderately larger than those of the backbone amides (∼150 ppm).[37] The asymmetry parameter η differs more significantly between the imidazole and amide nitrogens: η is ∼0.5 for imidazole NH groups but only 0.2 (i.e., nearly uniaxial) for backbone amides,[38] the latter due to the dominating influence of the carbonyl group on its electronic environment. Table 2 also shows that the middle

Table 2. ^{15}N CSA Principal Values, Anisotropy Parameters (δ), Asymmetry Parameters (η), and Spans ($\Delta\sigma$) in Histidine; Hydrogen-Bond Distances Are Also Included

state	site	δ_{iso} (ppm)	δ_{33} (ppm)	δ_{22} (ppm)	δ_{11} (ppm)	δ (ppm)	η	$\Delta\sigma$ (ppm)	H-bond (Å)
cationic	Nδ1—H	190	71	219	280	−119	0.51	209	2.63 [a]
	Nε2—H	176	63	195	270	−113	0.66	207	2.81 [a]
neutral τ tautomer	Nδ1	249	39	319	389	−210	0.33	350	2.76 [b]
	Nε2—H	171	73	184	256	−98	0.73	183	2.76 [b]
anionic τ tautomer	Nδ1	253	100	288	371	−153	0.54	271	−
	Nε2—H	167	71	175	255	−96	0.83	184	−
anionic π tautomer	Nδ1—H	172	69	189	258	−103	0.67	189	−
	Nε2	248	101	271	362	−147	0.62	261	−

[a] The cationic histidine hydrogen-bonding distances are based on the crystal structure of histidine hydrochloride monohydrate C$_6$H$_{12}$ClN$_3$O$_3$, measured on the pH 4.5 sample. [b] The distances for the neutral τ tautomer are R_{NN}, based on the crystal structure of histidine C$_6$H$_9$N$_3$O$_2$, measured on the pH 8.5 sample.
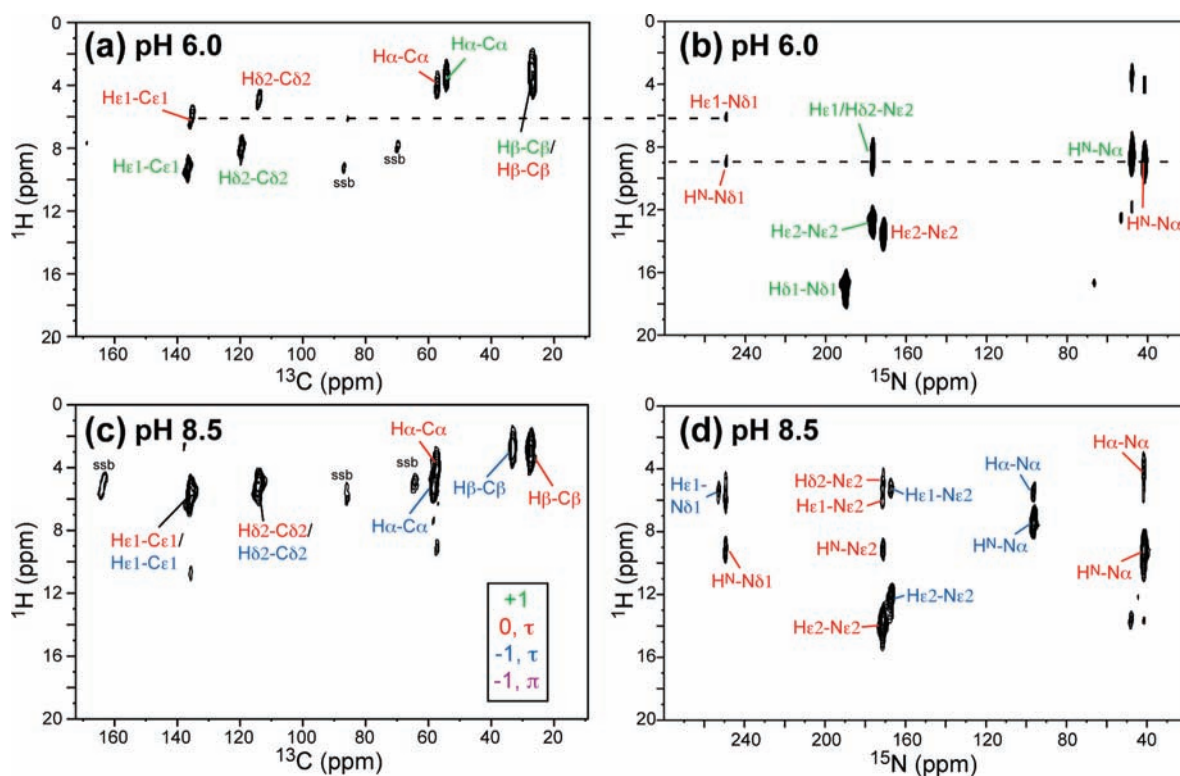

Figure 3. ^{1}H chemical shifts of histidine from 2D ^{1}H−^{13}C and ^{1}H−^{15}N HETCOR spectra: (a,b) His6.0; (c,d) His8.5; (a,c) ^{1}H−^{13}C HETCOR spectra; (b,d) ^{1}H−^{15}N HETCOR spectra. At both pH values, a mixture of two states was observed. Note the large downfield ^{1}H chemical shifts of Nδ1 in cationic histidine.

principal value, δ_{22}, ranges from 175 to 219 ppm for the protonated imidazole nitrogens. This principal value was known to be sensitive to H-bond formation:[17] δ_{22} shifts downfield by ∼50 ppm as R_{NO} decreases from 3.0 to 2.5 Å. We found Nδ1−H in the cationic histidine to exhibit the most downfield δ_{22} value (219 ppm), suggesting that it was involved in the strongest H-bond among all imidazole nitrogens.

Unprotonated imidazole nitrogens have much larger CSA spans of 260−350 ppm.[16,34] The CSA tensor orientation is known to differ between the unprotonated and protonated imidazole nitrogens: the direction of the most deshielded element, δ_{11}, is tangential to the ring for unprotonated nitrogens but radial to the ring in protonated nitrogens.[34] Density functional theory calculations suggested that the most downfield principal axis was sensitive to intermolecular H-bonding.[34] Table 2 shows that the unprotonated nitrogen in the neutral histidine has a significantly larger span (∼350 ppm) than the unprotonated nitrogens (∼270 ppm) in either tautomer of the anionic histidine. Below we examine the origin of this CSA difference by detecting intra- and intermolecular H-bonding through ^{1}H chemical shifts and N−H bond lengths.

^{1}H Chemical Shifts and Hydrogen Bonding. ^{1}H chemical shifts provide a sensitive indicator of the chemical structure and H-bonding of imidazoles. The ^{1}H isotropic chemical shift is well known to increase (move downfield) with increasing H-bond strength.[39,40] We measured the ^{1}H chemical shifts using 2D ^{1}H−^{13}C and ^{1}H−^{15}N HETCOR experiments. LG-CP was used to transfer the ^{1}H polarization to ^{13}C or ^{15}N in a site-specific fashion, and strong ^{1}H homonuclear decoupling was applied during t_1 to ensure site resolution and to prevent ^{1}H spin diffusion.[26] Figure 3 shows the HETCOR spectra of His6.0 and His8.5, where narrow line widths of 0.8 ± 0.3 ppm were observed in the ^{1}H dimension. At pH 6, where the cationic imidazolium (green) coexists with the neutral τ tautomer (red), the carbon-bonded Hδ2 and Hε1 resonate ~3 ppm downfield in the cationic histidine compared to those in the neutral τ tautomer (Figure 3a), which can be attributed to the delocalized positive charge creating a more deshielded environment for the protons. In the ^{15}N-detected HETCOR spectrum (Figure 3b), the unprotonated Nδ1 exhibits cross peaks both with Hε1 two bonds away and with the backbone NH$_3$. The amino ^{1}H chemical shift is 0.5 ppm more downfield in the neutral τ tautomer (9.1 ppm) than in the cationic imidazolium (8.6 ppm), supporting the existence of a NH$_3\cdots$Nδ1 H-bond.

At pH 8.5, where both neutral (red) and anionic (blue) τ tautomers exist, most aliphatic and aromatic ^{1}H's exhibit similar chemical shifts between the two states (Figure 3c,d). The main exceptions are the backbone NH$_3$ and side-chain Hε2 protons, which show lower chemical shifts in the anionic than in the neutral histidine. In addition, a cross peak between the unprotonated Nδ1 and backbone H^N was detected for the neutral τ tautomer, suggesting side chain−backbone H-bonding in the neutral histidine but not in the anionic histidine.

In general, unprotonated imidazole nitrogens can serve as H-bond acceptors, while the protonated nitrogens can act as H-bond donors. For the latter, the H-bond acceptors can be either backbone carbonyl or water molecules. To determine whether H-bonds indeed exist between water and Nδ1−H or Nε2−H, we measured ^{15}N-detected MELODI-HETCOR spectra. This experiment eliminates the signals of immobile ^{1}H spins directly bonded to a ^{13}C or ^{15}N spin by ^{13}C and ^{15}N dipole dephasing, thus ensuring that only water protons or dynamic protons can give rise to cross peaks in the 2D spectra. Figure 4 shows ^{15}N-detected MELODI-HETCOR spectra of His6.0 without (a) and with (b) dipolar dephasing pulses. The control spectrum exhibited the expected cross peaks between ^{15}N and aliphatic, amino, and water protons, while in the ^{13}C and ^{15}N-dephased spectrum, the signals of the aliphatic and aromatic protons were completely removed, leaving only water and mobile NH$_3$ signals. Interestingly, the spectrum shows that only the cationic histidine has cross peaks with water, while the neutral τ tautomer does not. These results agree with the crystal structures, which showed four water molecules in the unit cell of cationic histidine but no water molecules in neutral histidine (Figure S3, Supporting Information). The spectra confirm that the protonated and neutral molecules at pH 6 are not in molecular contact but pack in separate microcrystalline environments.

N−H Bond Lengths and Hydrogen Bond Formation. ^{15}N−^{1}H bond lengths provide an independent probe of the presence of H-bonds in histidine. Hydrogen bonding stretches the N−H bond from 1.05 Å[41] and thus reduces the N−H dipolar coupling from the rigid-limit covalent-bond value of 10 kHz.[18] Figure 5 shows the N−H DIPSHIFT results of Nδ1 and Nε2 in all four histidines. Among the protonated nitrogens, Nδ1 of the
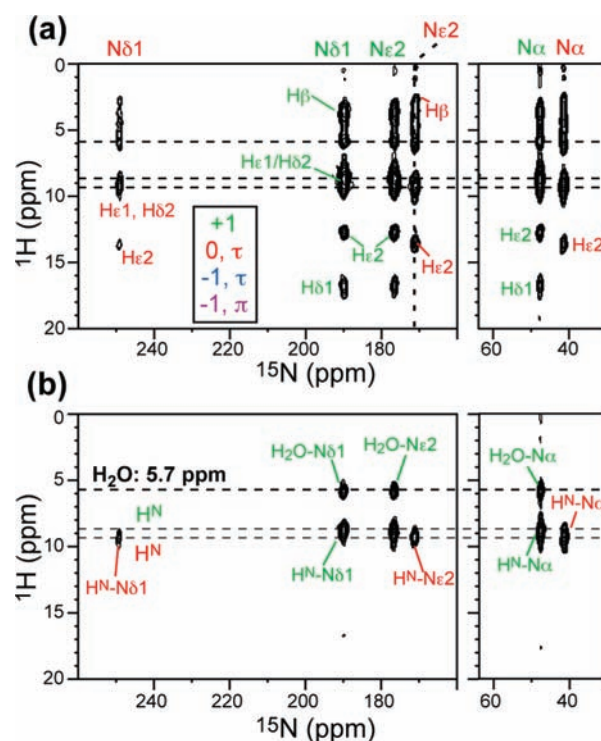

Figure 4. 2D ^{1}H−^{15}N MELODI-HETCOR spectra of His6.0 to identify intermolecular water−histidine hydrogen bonding. (a) Control spectrum without dipolar filter. (b) Spectrum with two rotor periods of ^{13}C and ^{15}N dipolar dephasing. Only water protons and mobile protons remain in (b).

cationic histidine exhibited the longest N−H bond of 1.09 Å, while Nε2 in the same sample exhibited a modestly increased bond length of 1.06 Å. In comparison, the imidazole nitrogens in the neutral and anionic histidines showed unstretched bond lengths of 1.05 Å. The prominent Nδ1−H bond stretching in cationic histidine is in excellent agreement with its large downfield ^{15}N δ_{22} principal value of 219 ppm (Table 2), its significantly downfield Hδ1 isotropic shift of 16.8 ppm (Figure 3b), and the presence of a strong Nδ1−water cross peak of the sample in the 2D MELODI-HETCOR spectrum (Figure 4b). Indeed, the crystal structure of histidine at pH 4.5 showed a short R_{NO} of 2.63 Å (Table 2), indicating a strong H-bond. In comparison, Nε2 in the same cationic histidine displayed a less robust panel of H-bonding effects: the ^{15}N δ_{22} principal value (195 ppm) and the Hε2 chemical shift (12.6 ppm) are not as far downfield, and the N−H bond stretching is modest (1.06 Å). Consistently, the crystal structure indicates a 0.2 Å longer R_{NO} distance of 2.81 Å for Nε2 (Table 2).

The different N−H bond lengths of protonated nitrogens between the cationic and neutral histidines can be understood on the basis of the different proton affinities of these histidines. According to a recent DFT calculation,[42] the proton affinity of Nδ1 and Nε2 ranged from −250 to −230 kcal/mol in cationic histidine but from −340 to −360 kcal/mol in neutral histidine. Thus, the protons in the cationic imidazolium are more easily removed than protons in the neutral imidazole.

For unprotonated nitrogens, the N−H dipolar couplings are much weaker, as expected. Since there are several proximal protons contributing to the observed couplings, the nearest-neighbor distance to a proton determined from the dipolar couplings should be systematically smaller than the true nearest-neighbor distance.
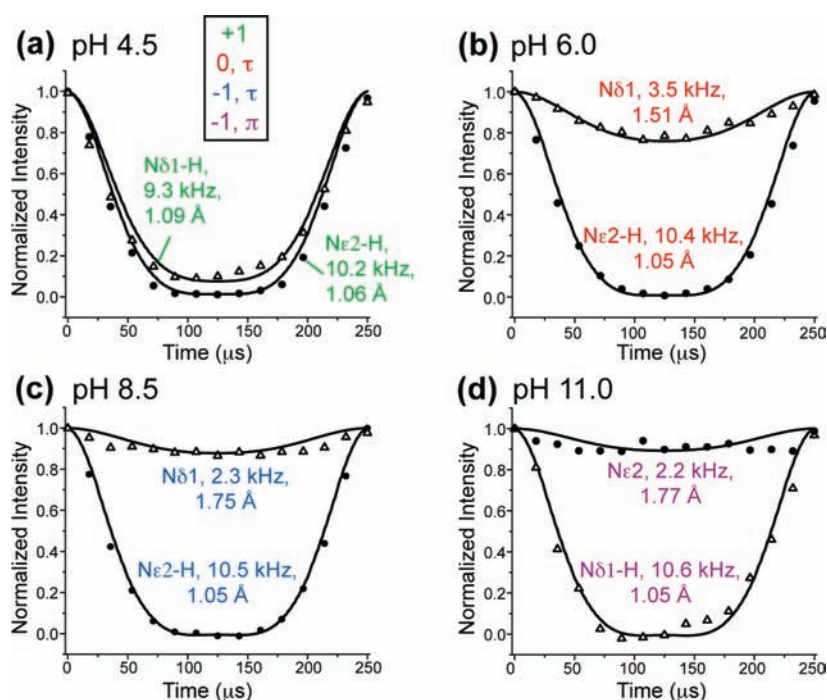
Figure 5. Nδ1 and Nε2 ^{15}N$-^1$H dipolar couplings of histidine as a function of pH and tautomeric structure. The dipolar dephasing curves are extracted from the t_1 dimension of 2D DIPSHIFT spectra. (a) Cationic histidine at pH 4.5. (b) Neutral τ tautomer at pH 6. (c) Anionic τ tautomer at pH 8.5. (d) Anionic π tautomer at pH 11. The coupling strengths and N$-$H distances are indicated.

Table 3. N$-$H Bond Length (R_{NH}) in Different Protonated and Tautomeric States of Histidine Determined from N$-$H Dipolar Couplings (ω_{NH})

sample	state	site	δ_N (ppm)	ω_{NH} (kHz)^a	R_{NH} (Å)
His4.5	cationic	Nδ1$-$H	190.0	9.3 $\pm$ 0.1	1.09 $\pm$ 0.01
		Nε2$-$H	176.3	10.2 $\pm$ 0.1	1.06 $\pm$ 0.01
His6.5	neutral τ	Nδ1	249.4	3.5 $\pm$ 0.1	1.51 $\pm$ 0.06
	tautomer	Nε2$-$H	171.1	10.4 $\pm$ 0.2	1.05 $\pm$ 0.02
His8.5	anionic τ	Nδ1	252.7	2.3 $\pm$ 0.4	1.75 $\pm$ 0.20
	tautomer	Nε2$-$H	167.3	10.5 $\pm$ 0.1	1.05 $\pm$ 0.01
His11.0	anionic π	Nδ1$-$H	171.8	10.6 $\pm$ 0.3	1.05 $\pm$ 0.02
	tautomer	Nε2	248.2	2.2 $\pm$ 0.3	1.77 $\pm$ 0.25

^{a} A FSLG scaling factor of 0.540 was measured from model compound experiments and used in fitting the N$-$H dipolar couplings.

Between pH 6 and 11, the strongest dipolar coupling was found for Nδ1 (3.5 kHz) in the neutral τ tautomer at pH 6, corresponding to an effective N$-$H distance of 1.51 Å (Table 3). This distance suggests a strong H-bond, possibly with the backbone amino group, because of the clear H$^N-$Nδ1 cross peak in the 2D ^{1}H$-^{15}$N HETCOR spectra at pH 6 and 8.5 (Figure 3b,d). In comparison, the unprotonated Nδ1 in the anionic τ tautomer (pH 8.5) showed a significantly weaker dipolar coupling of 2.3 kHz, consistent with the lack of a backbone NH$_2$ cross peak with Nδ1 in the HETCOR spectrum (Figure 3d).

χ_1 and χ_2 Torsion Angles from Backbone$-$Side Chain Distances. The side-chain conformation of histidines in proteins has important implications for protein function. We now demonstrate that it is possible to measure the side-chain χ_1 and χ_2 angles accurately. A number of methods have been introduced to determine the side-chain rotameric structure of amino acids: for example, direct dipolar correlation techniques such as HCCH are useful for β-branched amino acids,[43] and methyl ^{13}C chemical shifts of doubly methylated amino acid residues (Val, Leu, and Ile) are sensitive to the side-chain conformation.[44] Here we chose to measure backbone$-$side chain ^{13}C$-^{15}$N distances, using the frequency-selective REDOR technique,[31,45] to quantify the χ_1 and χ_2 angles.

The Cα-to-imidazole ^{15}N distances depend on the χ_2 angle, and the Nα-to-side-chain carbon distances depend on both χ_1 and χ_2 angles (Figure 6), according to the following equations:

$$d^2_{C\alpha-N\delta1} = (d_{C\gamma N\delta1} \sin \chi_2 \sin 120°)^2$$
$$+ (-d_{C\alpha C\beta} \sin 109° + d_{C\gamma N\delta1} \cos \chi_2 \sin 120°)^2$$
$$+ (-d_{C\alpha C\beta} \cos 109° + d_{C\beta C\gamma} - d_{C\gamma N\delta1} \cos 120°)^2 \quad (4)$$

$$d^2_{C\alpha-N\varepsilon2} = [d_{C\gamma N\varepsilon2} \sin(\chi_2 - 180°) \sin \theta_1]^2$$
$$+ [-d_{C\alpha C\beta} \sin 109° + d_{C\gamma N\varepsilon2} \cos(\chi_2 - 180°) \sin \theta_1]^2$$
$$+ (-d_{C\alpha C\beta} \cos 109° + d_{C\beta C\gamma} - d_{C\gamma N\varepsilon2} \cos \theta_1)^2 \quad (5)$$

$$d^2_{C\delta2-N\alpha} = [d_{N\alpha C\alpha} \sin \chi_1 \sin 109°$$
$$- d_{C\gamma C\delta2} \sin(\chi_2 - 180°)\sin 120°]^2 + [d_{C\alpha C\beta} - d_{N\alpha C\alpha} \cos 109°$$
$$- (d_{C\beta C\gamma} - d_{C\gamma C\delta2} \cos 120°) \cos 109°$$
$$+ d_{C\gamma C\delta2} \sin 120° \cos(\chi_2 - 180°) \sin 109°)]^2$$
$$+ [-d_{N\alpha C\alpha} \sin 109° \cos \chi_1 + d_{C\beta C\gamma} \sin 109°$$
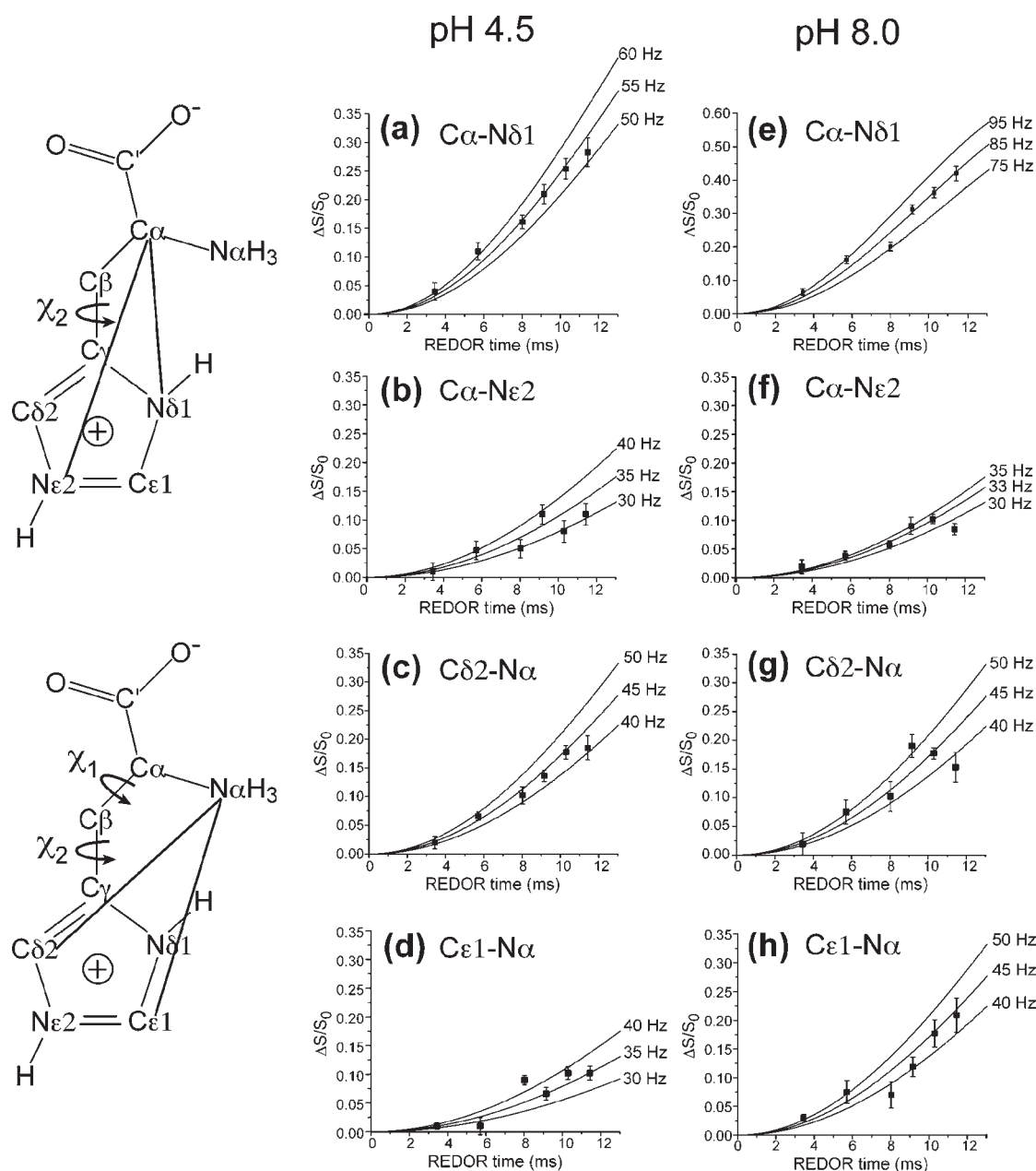$$- d_{C\gamma C\delta2} \cos 109° \cos(\chi_2 - 180°) \sin 120°]^2 \quad (6)$$

Figure 6. Intramolecular $^{13}C-^{15}N$ distances between the side chain and backbone of histidine to determine (χ_1, χ_2) angles: (a−d) cationic histidine at pH 4.5; (e−h) neutral τ tautomer at pH 8.0; (a,e) $C\alpha-N\delta1$ REDOR data; (b,f) $C\alpha-N\varepsilon2$ REDOR data; (c,g) $C\delta2-N\alpha$ REDOR data; (d,h) $C\varepsilon1-N\alpha$ REDOR data. Left: Schematic representation of the χ_2-dependent $C\alpha-N\delta1$ and $C\alpha-N\varepsilon2$ distances and the (χ_1, χ_2)-dependent $C\delta2-N\alpha$ and $C\varepsilon1-N\alpha$ distances.

$$d^2_{C\varepsilon1-N\alpha} = [d_{N\alpha C\alpha} \sin \chi_1 \sin 109° + d_{C\gamma C\varepsilon1} \sin \chi_2 \sin \theta_2]^2$$
$$+ [d_{C\alpha C\beta} - d_{N\alpha C\alpha} \cos 109° - (d_{C\beta C\gamma} - d_{C\gamma C\varepsilon1} \cos \theta_2) \cos 109°$$
$$+ d_{C\gamma C\varepsilon1} \sin \theta_2 \cos \chi_2 \sin 109°)]^2$$
$$+ [- d_{N\alpha C\alpha} \sin 109° \cos \chi_1 + d_{C\beta C\gamma} \sin 109°$$
$$- d_{C\gamma C\varepsilon1} \cos 109° \cos \chi_2 \sin \theta_2]^2 \qquad (7)$$

In eqs 4−7, the bond lengths and covalently fixed two-bond distances (d's) were set to crystallographic values for histidine hydrochloride monohydrate (HISTCM12, Cambridge Structure Database). The bond angles were 109° for $\angle N\alpha C\alpha C\beta$ and $\angle C\alpha C\beta C\gamma$ and 120° for $\angle C\beta C\gamma N\delta1$, $\angle C\beta C\gamma C\delta2$, and $\angle C\beta C\gamma C\varepsilon1$. The angles $\angle C\beta C\gamma N\varepsilon2$ (θ_1) and $\angle C\beta C\gamma C\varepsilon1$ (θ_2) were also fixed by the covalent geometry to be 166.7° and 157.2°, respectively.

Figure 6 shows the $^{13}C-^{15}N$ REDOR $\Delta S/S_0$ curves of 20% diluted histidine at pH 4.5 and 8.0. Significant differences were observed between the two samples for the $C\alpha-N\delta1$ and $C\varepsilon1-N\alpha$ couplings, indicating that the χ_1 and χ_2 angles differ between the cationic and neutral histidines. The resulting intramolecular distances (Table 4) agree well with the crystal structure, within ±0.2 Å, for most sites. The largest deviation was observed for the $C\alpha-N\delta1$ distance in the neutral τ tautomer: the NMR distance was longer by 0.3 Å than the crystal structure value. This may be partly due to the large ^{15}N CSA of this unprotonated site, even

Table 4. ^{13}C$-^{15}$N Intramolecular Distances and Side-Chain (χ_1, χ_2) Angles in Cationic and Neutral τ Tautomer of Histidine

| state | method | intramolecular distance (Å) | | | | χ_1 | χ_2 |
		Cα−Nδ1	Cα−Nε2	Cδ2−Nα	Cε1−Nα		
cationic	SSNMR	3.84 ± 0.20	4.46 ± 0.20	4.10 ± 0.20	4.70 ± 0.20	75	−120
						−75	120
	X-ray[a]	3.64	4.47	3.95	4.77	72.0	−121.1
neutral τ tautomer	SSNMR	3.32 ± 0.20	4.55 ± 0.20	4.10 ± 0.20	4.10 ± 0.20	−55	60
						55	−60
	X-ray[b]	3.06	4.57	4.24	4.00	−58.3	56.1

[a] These distances were extracted from the crystal structure of histidine hydrochloride monohydrate $C_6H_{12}ClN_3O_3$, measured on the pH 4.5 sample.
[b] These distances were extracted from the crystal structure of histidine $C_6H_9N_3O_2$, measured on the pH 8.5 sample.
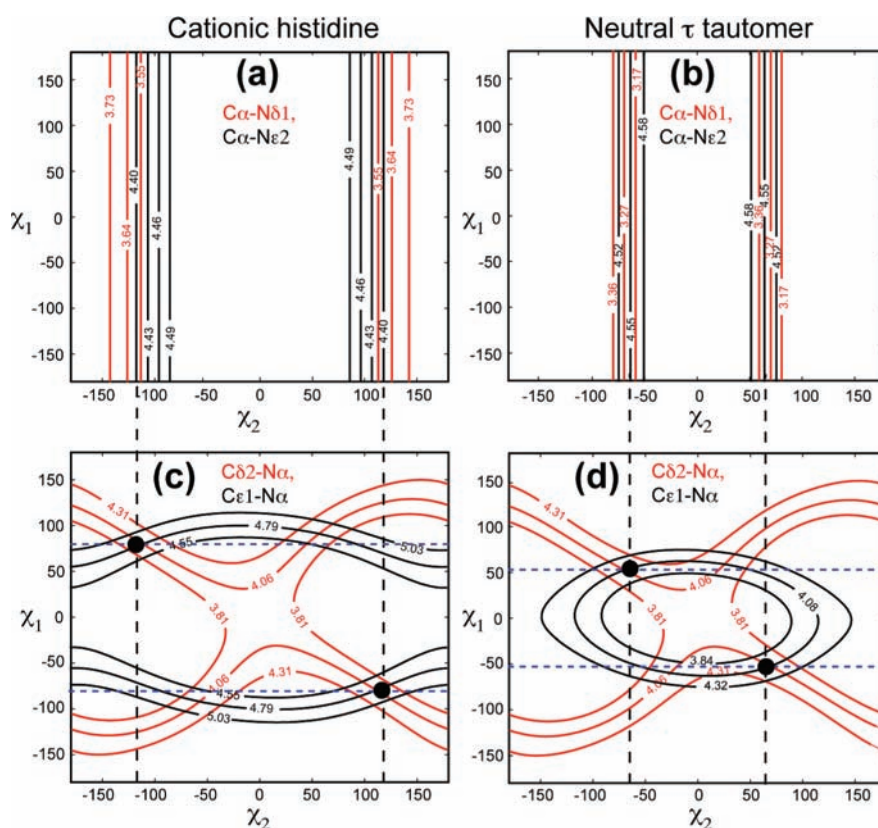

Figure 7. Contour plots of intramolecular ^{13}C$-^{15}$N distances as a function of (χ_1, χ_2) torsion angles. Only contour lines matching the measured distance values are shown. (a,b) Measured Cα−Nδ1 (red) and Cα−Nε2 (black) distances for cationic imidazolium at pH 4.5 (a) and neutral τ tautomer at pH 8.5 (b). (c,d) Measured Cδ2−Nα (red) and Cε1−Nα (black) distances in cationic histidine (c) and neutral τ tautomer (d). Best-fit torsion angles were read from the positions where the contours overlap.

though SIMPSON simulations were carried out to include the CSA effect.

The backbone−side chain ^{13}C$-^{15}$N distances were converted to (χ_1, χ_2) angles according to eqs 4−7. Figure 7 shows contour plots of distances as a function of (χ_1, χ_2) angles. The overlap between the Cα−Nδ1 and Cα−Nε2 distance contours constrains the χ_2 angle, while the overlap between the Cδ2−Nα and Cε1−Nα distances constrains both χ_1 and χ_2 angles. The availability of multiple distances reduced the degeneracy of the dihedral angles to two. Cationic histidine yielded (χ_1, χ_2) angles of ($-75°, +120°$) or ($+75°, -120°$), the second set of values being within 3° of the crystal structure values obtained on the

same compound. For the neutral τ tautomer, the best-fit (χ_1, χ_2) angles were ($-55°, +60°$) or ($+55°, -60°$), the first set of values agreeing with the crystal structure values to ±4°. Thus, the backbone−side chain ^{13}C$-^{15}$N distances can be measured accurately to determine the side-chain rotameric conformation, and the experiments are applicable to proteins to determine functionally important rotameric structures of histidines.[11]

■ CONCLUSIONS

The protonation state, tautomeric structure, hydrogen bonding, and rotameric structures of histidines were comprehensively

investigated in a wide pH range using MAS solid-state NMR techniques. Two-dimensional correlation experiments resulted in a complete set of ^{1}H, ^{13}C, and ^{15}N isotropic chemical shifts for four states of histidine: the cationic histidine, the neutral τ tautomer, and the anionic τ and π tautomers. The ^{15}N and ^{13}C chemical shifts are sensitive to both the protonation state and the tautomeric structure, while ^{15}N and ^{1}H chemical shifts are sensitive to hydrogen bonding of the imidazole ring. Multiple lines of evidence, including heteronuclear correlation spectra, N—H bond length, and ^{15}N CSA, consistently indicate strong H-bonds between the protonated Nδ1 and water in the cationic but not the neutral histidine. Hydrogen bonding was also observed between backbone NH$_3$ and unprotonated Nδ1 in the neutral τ tautomer, with a measured $R_{N\cdots H}$ distance of 1.5 Å. The side-chain dihedral angels χ_1 and χ_2 can be accurately measured, to within 4° of the crystal structure value, through backbone—side chain ^{13}C—^{15}N distances. These results extend our knowledge of the influence of histidine chemical structure and three-dimensional structure on NMR parameters, and provide a large panel of benchmark values to facilitate the study of the high-resolution structure, dynamics, and pH-dependent chemistry of histidines in proteins.

■ ASSOCIATED CONTENT

Ⓢ Supporting Information. Additional isotropic and ^{15}N recoupled anisotropic chemical shift spectra and crystal structures of histidine at different pH values. This material is available free of charge via the Internet at http://pubs.acs.org.

■ AUTHOR INFORMATION

Corresponding Author
mhong@iastate.edu

■ ACKNOWLEDGMENT

■ REFERENCES

(1) Strothkamp, K. G.; Lippard, S. J. *Acc. Chem. Res.* **1982**, *15*, 318–326.

(2) Morgan, J. E.; Verkhovsky, M. I.; Wikström, M. *J. Bioenerg. Biomembr.* **1994**, *26*, 599–608.

(3) Cleland, W. W. *Arch. Biochem. Biophys.* **2000**, *382*, 1–5.

(4) Bachovchin, W. W.; Roberts, J. D. *J. Am. Chem. Soc.* **1978**, *100*, 8041–8047.

(5) Cady, S. D.; Luo, W. B.; Hu, F.; Hong, M. *Biochemistry* **2009**, *48*, 7356–7364.

(6) Wang, C.; Lamb, R. A.; Pinto, L. H. *Biophys. J.* **1995**, *69*, 1363–1371.

(7) Brzezinski, P.; Gennis, R. B. *J. Bioenerg. Biomembr.* **2008**, *40*, 521–531.

(8) Diner, B. A. *Biochim. Biophys. Acta* **2001**, *1503*, 147–163.

(9) Stockel, J.; Safar, J.; Wallace, A. C.; Cohen, F. E.; Prusiner, S. B. *Biochemistry* **1998**, *37*, 7185–7193.

(10) Atwood, C. S.; Moir, R. D.; Huang, X. D.; Scarpa, R. C.; Bacarra, N. M. E.; Romano, D. M.; Hartshorn, M. K.; Tanzi, R. E.; Bush, A. I. *J. Biol. Chem.* **1998**, *273*, 12817–12826.

(11) Hu, F.; Luo, W.; Hong, M. *Science* **2010**, *330*, 505–508.

(12) Alia; Matysik, J.; Soede-Huijbregts, C.; Baldus, M.; Raap, J.; Lugtenburg, J.; Gast, P.; van Gorkom, H. J.; Hoff, A. J.; de Groot, H. J. M. *J. Am. Chem. Soc.* **2001**, *123*, 4803–4809.

(13) Hass, M. A. S.; Hansen, D. F.; Christensen, H. E. M.; Led, J. J.; Kay, L. E. *J. Am. Chem. Soc.* **2008**, *130*, 8460–8470.

(14) Hu, J.; Fu, R.; Nishimura, K.; Zhang, L.; Zhou, H. X.; Busath, D. D.; Vijayvergiya, V.; Cross, T. A. *Proc. Natl. Acad. Sci. U.S.A.* **2006**, *103*, 6865–6870.

(15) Harbison, G.; Herzfeld, J.; Griffin, R. G. *J. Am. Chem. Soc.* **1981**, *103*, 4752–4754.

(16) Munowitz, M.; Bachovchin, W. W.; Herzfeld, J.; Dobson, C. M.; Griffin, R. G. *J. Am. Chem. Soc.* **1982**, *104*, 1192–1196.

(17) Wei, Y. F.; de Dios, A. C.; McDermott, A. E. *J. Am. Chem. Soc.* **1999**, *121*, 10389–10394.

(18) Song, X. J.; Rienstra, C. M.; McDermott, A. E. *Magn. Reson. Chem.* **2001**, *39*, S30–S36.

(19) Henry, B.; Tekely, P.; Delpuech, J. J. *J. Am. Chem. Soc.* **2002**, *124*, 2025–2034.

(20) Cheng, F.; Sun, H. H.; Zhang, Y.; Mukkamala, D.; Oldfield, E. *J. Am. Chem. Soc.* **2005**, *127*, 12544–12554.

(21) Rienstra, C. M.; Tucker-Kellogg, L.; Jaroniec, C. P.; Hohwy, M.; Reif, B.; McMahon, M. T.; Tidor, B.; Lozano-Perez, T.; Griffin, R. G. *Proc. Natl. Acad. Sci. U.S.A.* **2002**, *99*, 10260–10265.

(22) Takegoshi, K.; Nakamura, S.; Terao, T. *Chem. Phys. Lett.* **2001**, *344*, 631–637.

(23) Hong, M.; Griffin, R. G. *J. Am. Chem. Soc.* **1998**, *120*, 7113–7114.

(24) Gullion, T.; Schaefer, J. *J. Magn. Reson.* **1989**, *81*, 196–200.

(25) Lee, M.; Goldburg, W. I. *Phys. Rev.* **1965**, *140*, A1261.

(26) Bielecki, A.; Kolbert, A. C.; Levitt, M. H. *Chem. Phys. Lett.* **1989**, *155*, 341–346.

(27) Li, S. H.; Su, Y. C.; Luo, W. B.; Hong, M. *J. Phys. Chem. B* **2010**, *114*, 4063–4069.

(28) Yao, X. L.; Schmidt-Rohr, K.; Hong, M. *J. Magn. Reson.* **2001**, *149*, 139–143.

(29) Liu, S. F.; Mao, J. D.; Schmidt-Rohr, K. *J. Magn. Reson.* **2002**, *155*, 15–28.

(30) Hong, M.; Gross, J. D.; Rienstra, C. M.; Griffin, R. G.; Kumashiro, K. K.; Schmidt-Rohr, K. *J. Magn. Reson.* **1997**, *129*, 85–92.

(31) Jaroniec, C. P.; Tounge, B. A.; Herzfeld, J.; Griffin, R. G. *J. Am. Chem. Soc.* **2001**, *123*, 3507–3519.

(32) Sinha, N.; Schmidt-Rohr, K.; Hong, M. *J. Magn. Reson.* **2004**, *168*, 358–365.

(33) Bak, M.; Rasmussen, T.; Nielsen, N. C. *J. Magn. Reson.* **2000**, *147*, 296–330.

(34) Solum, M. S.; Altmann, K. L.; Strohmeier, M.; Berges, D. A.; Zhang, Y. L.; Facelli, J. C.; Pugmire, R. J.; Grant, D. M. *J. Am. Chem. Soc.* **1997**, *119*, 9804–9809.

(35) Haddad, K. C.; Sudmeier, J. L.; Bachovchin, D. A.; Bachovchin, W. W. *Proc. Natl. Acad. Sci. U.S.A.* **2005**, *102*, 1006–1011.

(36) Poon, A.; Birn, J.; Ramamoorthy, A. *J. Phys. Chem. B* **2004**, *108*, 16577–16585.

(37) Wylie, B. J.; Sperling, L. J.; Frericks, H. L.; Shah, G. J.; Franks, W. T.; Rienstra, C. M. *J. Am. Chem. Soc.* **2007**, *129*, 5318–5319.

(38) Wu, C. H.; Ramamoorthy, A.; Gierasch, L. M.; Opella, S. J. *J. Am. Chem. Soc.* **1995**, *117*, 6148–6149.

(39) Berglund, B.; Vaughan, R. W. *J. Chem. Phys.* **1980**, *73*, 2037–2043.

(40) Yao, L.; Grishaev, A.; Cornilescu, G.; Bax, A. *J. Am. Chem. Soc.* **2010**, *132*, 10866–10875.

(41) Roberts, J. E.; Harbison, G. S.; Munowitz, M. G.; Herzfeld, J.; Griffin, R. G. *J. Am. Chem. Soc.* **1987**, *109*, 4163–4169.

(42) Hudaky, P.; Perczel, A. *J. Phys. Chem. A* **2004**, *108*, 6195–6205.

(43) Feng, X.; Eden, M.; Brinkmann, A.; Luthman, H.; Eriksson, L.; Graslund, A.; Antzutkin, O. N.; Levitt, M. H. *J. Am. Chem. Soc.* **1997**, *119*, 12006–12007.

(44) Hong, M.; Mishanina, T. V.; Cady, S. D. *J. Am. Chem. Soc.* **2009**, *131*, 7806–7816.

(45) Jaroniec, C. P.; Filip, C.; Griffin, R. G. *J. Am. Chem. Soc.* **2002**, *124*, 10728–10742.